https://doi.org/10.5194/egusphere-2023-2427
Preprint. Discussion started: 18 December 2023

Using historical temperature to constrain the climate sensitivity and aerosol-induced cooling

Olaf Morgenstern[1]

[1]National Institute of Water and Atmospheric Research (NIWA), Wellington, New Zealand

Correspondence: Olaf Morgenstern (olaf.morgenstern@niwa.co.nz)

Abstract. The most recent generation of climate models that has informed the 6$^{\text{th}}$ Assessment Report (AR6) of IPCC is characterized by the presence of several models with anomalously large equilibrium climate sensitivities (ECSs) relative to the previous generation. Partly as a result, AR6 did not use any direct quantifications of ECSs using $4\times CO_2$ simulations and relied on other evidence when assessing the Earth's actual ECS. Here I use the historical observed global-mean surface air temperature and simulations produced under the Detection and Attribution Model Intercomparison Project to constrain the ECS and historical aerosol-related cooling. Based on 15 largely independent models I obtain an average adjusted ECS of 3.4$\pm$0.8 K (at 68% confidence), which is very consistent with the AR6 estimate. Furthermore, importantly I find that the optimal cooling due to anthropogenic aerosols consistent with the observed temperature record should on average be about 34$\pm$31% of what these models simulate, yielding an aerosol-related global-mean cooling for 2000-2014, relative to 1850-1899, of -0.19 ± 0.14 K (at 68% confidence), when these models simulate on average -0.63 ± 0.28 K. For 12 models the reduction in aerosol-related cooling equals or exceeds 50%. There is a correlation between the models' ECS and their aerosol-related cooling, whereby large-ECS models tend to be associated also with large aerosol-related cooling. The results imply that a large reduction of the aerosol-related cooling, along with a more moderate adjustment of the greenhouse-gas related warming, for most models would bring the historical global mean temperature simulated by these models into better agreement with observations.

1 Introduction

The equilibrium climate sensitivity (ECS) is a well-established (Arrhenius, 1896) yet, despite progress, poorly constrained property of the climate system (Knutti et al., 2017; Forster et al., 2021; Smith and Forster, 2021). For a hypothetical doubling of the atmospheric CO_2 content above preindustrial levels, it states the associated surface temperature increase at equilibrium. Disagreement amongst climate models, particularly in the most recent generation of climate models (Meehl et al., 2020), is an impediment to narrowing its associated long-standing uncertainty. The large spread in ECSs characterizing the present generation of climate models is contributing to some substantial inter-model spread in simulated end-of-century warming in future-scenario simulations (Lee et al., 2021). It is therefore desirable to reduce this model disagreement to more confidently project future climate under any climate scenario.

In this work I explore what "historical", all-forcings experiments and single-forcing experiments conducted for the Detection and Attribution Model Intercomparison Project (DAMIP, Gillett et al., 2016) imply for both the climate sensitivity and

https://doi.org/10.5194/egusphere-2023-2427
Preprint. Discussion started: 18 December 2023

the aerosol-driven cooling which partially offsets global warming. GHG-driven warming and aerosol-induced cooling by far dominate the human influence on global-mean surface temperature (Forster et al., 2021). Decreases in future aerosol loading are thought to contribute to projected warming (Andreae et al., 2005), but the size of this feedback is highly uncertain (Forster et al., 2021; Watson-Parris and Smith, 2022). In individual models mismatches between observed and simulated "historical" global-mean surface temperatures have been associated with a misrepresentation of the aerosol-induced cooling (Andrews et al., 2020; Golaz et al., 2022), such that despite the increase in the mean ECS characterizing the 6$^{\text{th}}$ Coupled Model Intercomparison Project (CMIP6) ensemble of models, relative to CMIP5, the simulated historical warming in CMIP6 is actually smaller than in CMIP5 (Flynn and Mauritsen, 2020; Smith and Forster, 2021). Smith and Forster (2021) relate an increase in aerosol-driven cooling in CMIP6 versus CMIP5 to coupling to the also increased GHG-driven warming.

Below we develop a heuristic regression approach to evaluate, for all models participating in DAMIP, the fidelity of the simulation of both GHG-driven surface warming and aerosol-related cooling in the CMIP6 ensemble.

2 Data and Method

2.1 DAMIP models and experiments

Simulations produced for DAMIP, "historical" simulations (Eyring et al., 2016) extended to 2020 using the mid-range Shared Socioeconomic Pathway (SSP) 245 simulations (Gidden et al., 2019), and published ECS values that are based on 4×CO_2 simulations (Eyring et al., 2016) form the basis of this analysis.I use all 15 models for which "hist-GHG", "hist-aer", and "hist-nat" simulations are available (table 1). The hist-GHG, hist-aer, and hist-nat experiments are identical to the "historical", coupled all-forcings simulations except that forcings other than the GHGs, aerosols or their precursors, and natural (solar, volcanic) influences, respectively, are held at their 1850 values (Gillett et al., 2016).

The models that have completed these simulations span a large range of ECSs (between 2.4 and 5.6 K). For 12 models the simulation period for DAMIP simulations is 1850-2020, but three models (CESM2, E3SM-2-0, GISS-E2-1-G) end their DAMIP simulations in 2014. For these models I only use their "historical" temperature at the surface (tas) fields without extension.

Furthermore as an observational reference I use the HadCRUT5 global-mean surface temperature climatology (Morice et al., 2021). I form ensemble-, global-, and annual-mean temperature timeseries from the available simulations.

Figure 1 summarizes the behaviour of surface temperature in the 15 models over the historical period. Panel (a) indicates that as there is an approximate proportionality between the simulated warming attributable to GHGs (as taken from the hist-GHG ensembles) and the models' tabulated ECS values. Furthermore, panel (b) indicates that with some notable exceptions, the models are mostly additive in the sense that the sum of the warmings simulated in the three DAMIP ensembles is mostly quite similar to the warming simulated in the models' historical ensembles.

https://doi.org/10.5194/egusphere-2023-2427
Preprint. Discussion started: 18 December 2023

Table 1. DAMIP models, ensemble sizes of the experiments, literature ECS values of the models, and references for the ECS values and the model data.

Model	Sizes of ensembles (historical/hist-ghg/hist-aer/hist-nat/ssp245)	ECS (K)	Reference for ECS	References for data
ACCESS-CM2	10/3/3/3/5	4.7	Meehl et al. (2020)	Dix et al. (2019a, b, 2020a, b, c)
ACCESS-ESM1-5	40/3/3/3/40	3.9	Meehl et al. (2020)	Ziehn et al. (2019a, b, 2020a, b, c)
BCC-CSM2-MR	3/3/3/3/1	3.0	Meehl et al. (2020)	Wu et al. (2018, 2019a, b, c); Xin et al. (2019)
CanESM5	25/25/15/25/25	5.6	Meehl et al. (2020)	Swart et al. (2019a, b, c, d, e)
CESM2	11/3/2/3/0	5.2	Meehl et al. (2020)	Danabasoglu (2019a, b, c, 2020)
CNRM-CM6-1	30/10/10/10/10	4.8	Meehl et al. (2020)	Voldoire (2018, 2019a, b, c, d)
E3SM-2-0	5/5/5/5/0	4.0	Qin et al. (2023)	E3SM (2022a, b, c, d)
FGOALS-g3	6/3/3/3/4	2.8	Li et al. (2020)	Li (2019, 2020a, b, c, d)
GFDL-ESM4	3/1/1/3/3	3.9	Meehl et al. (2020)	Krasting et al. (2018); Horowitz et al. (2018a, b, c); John et al. (2018)
GISS-E2-1-G	10/5/5/5/0	2.4	Meehl et al. (2020)	NASA/GISS (2018a, b, c, d)
HadGEM3-GC31-LL	5/5/60/10/5	5.6	Meehl et al. (2020)	Ridley et al. (2019); Jones (2019a, b, c); Good (2019)
IPSL-CM6A-LR	33/10/10/10/11	4.6	Meehl et al. (2020)	Boucher et al. (2018a, b, c, d, 2019)
MIROC6	50/50/10/50/50	2.6	Meehl et al. (2020)	Tatebe and Watanabe (2018); Shiogama (2019a, b, c); Shiogama et al. (2019)
MRI-ESM2-0	10/3/3/3/5	3.2	Meehl et al. (2020)	Yukimoto et al. (2019a, b, c, d, e)
NorESM2-LM	3/3/3/3/3	2.5	Meehl et al. (2020)	Seland et al. (2019a, b, c, d, e)

2.2 Regression models

Using a linear regression approach, I derive rescaling factors α_1, β_1, γ_1, α_2, β_2, and γ_2 for the temperature responses to GHG, aerosol, and natural forcings such that the resultant sums of the rescaled simulated temperature anomalies minimize the root-mean-squared deviations ϵ_1 and ϵ_2 versus the ensemble-, global-, and annual-mean "historical" surface-air temperature anomaly T_{hist} and the HadCRUT5 temperature anomaly record T_{obs}, respectively, over the period 1920-2020 or 2014 (101 or 95 years), respectively:

$$T_{obs} = \alpha_1 T_{hGHG} + \beta_1 T_{haer} + \gamma_1 T_{hnat} + \epsilon_1 \text{ and} \quad (1)$$

$$T_{hist} = \alpha_2 T_{hGHG} + \beta_2 T_{haer} + \gamma_2 T_{hnat} + \epsilon_2. \quad (2)$$

T_{hGHG}, T_{haer} and T_{hnat} are all normalized relative to their 1850-1899 average. For a model which is perfectly additive in the anthropogenic GHG, anthropogenic aerosol, and natural forcings, and in the absence of climatological noise, the regression coefficients α_2, β_2, and γ_2 would be 1. For the purposes of comparison of these two regression models, I form the ratios of the

https://doi.org/10.5194/egusphere-2023-2427
Preprint. Discussion started: 18 December 2023

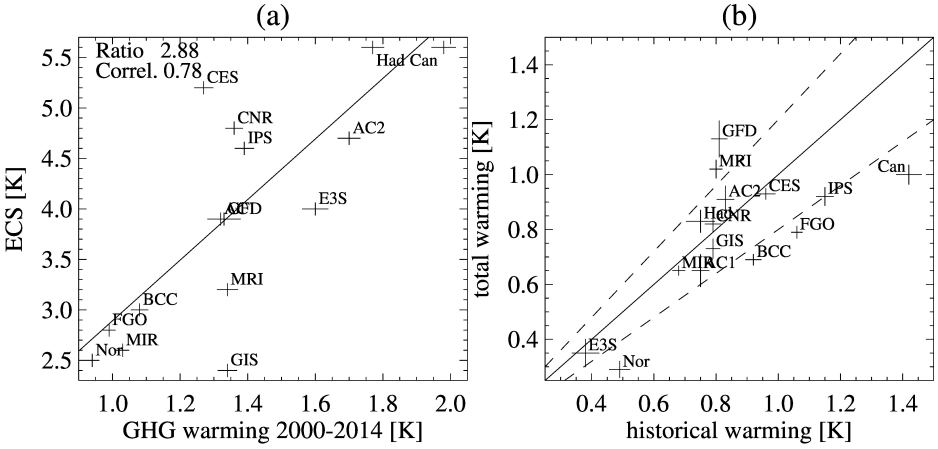

Figure 1. (a) Simulated global- and annual-mean warming for 2000-2014 in the hist-GHG ensembles of the DAMIP models, relative to the 1850-1899 mean, versus their ECSs (all in K). The width of the horizontal lines corresponds to std $(T_i)/\sqrt{15}$, where the T_i are the annual-mean temperatures for 2000-2014. Solid line: best-estimate proportional fit. The models' names are abbreviated to three characters. AC1 = ACCESS-ESM1-5. AC2 = ACCESS-CM2. (b) Simulated global-mean warming between 1850-1899 and 2000-2014 in the "historical" ensembles versus the sum of these warmings simulated in the respective hist-GHG, hist-aer, and hist-nat ensembles. The solid line marks the diagonal, dashed lines the 80 and 120% lines; the lengths of the bars in both directions correspond to the statistical uncertainties at 68% confidence.

regression coefficients

$$A = \frac{\alpha_1}{\alpha_2}, B = \frac{\beta_1}{\beta_2} \tag{3}$$

and their uncertainties

$$\delta A = A\sqrt{\left(\frac{\delta\alpha_1}{\alpha_1}\right)^2 + \left(\frac{\delta\alpha_2}{\alpha_2}\right)^2} \text{ and} \tag{4}$$

$$\delta B = B\sqrt{\left(\frac{\delta\beta_1}{\beta_1}\right)^2 + \left(\frac{\delta\beta_2}{\beta_2}\right)^2}, \tag{5}$$

where $\delta\alpha_1$ etc. are the single-variable uncertainties that emerge from the regression analysis.

I note that there is a considerable joint uncertainty resulting from substantial anticorrelations between T_{hGHG} and T_{haer}, but much smaller correlations (and practically no joint uncertainty) between T_{hGHG} and T_{nat}, and between T_{haer} and T_{nat}. This allows me to simplify the analysis and focus in the following only on the GHG and aerosol influences. To study their joint uncertainty, I calculate, as a function of α and β and time, the regression error timeseries

$$r_{obs}(\alpha,\beta) = T_{obs} - \alpha T_{GHG} - \beta T_{haer} - \gamma_1 T_{hnat} \tag{6}$$

https://doi.org/10.5194/egusphere-2023-2427
Preprint. Discussion started: 18 December 2023

I thus define an error function

$$E_{obs}(\alpha,\beta) \equiv \sqrt{\frac{\overline{r_{obs}^2(\alpha,\beta)}}{\overline{\epsilon_1^2}}}, \tag{7}$$

where the overbar denotes the 101 and 95-year means over 1920-2020 and 1920-2014, respectively.

I define that a regression fit differs from the optimal fit of equation 1 if $E_{obs} > E_{max}$, where E_{max} is a value of the error function, to be determined below, where the fits associated with such an RMS residual differ significantly from the optimal fit.

Substituting $Q_{obs}(\alpha,\beta) = \overline{r_{obs}^2(\alpha,\beta)}$, with $\Delta\alpha = \alpha - \alpha_1$ and $\Delta\beta = \beta - \beta_1$, I express Q_{obs} as a quadratic form expanded around the minimum:

$$Q_{obs}(\alpha,\beta) = \overline{\epsilon_1^2} + \frac{1}{2}(\Delta\alpha,\Delta\beta)\mathbf{M}\begin{pmatrix}\Delta\alpha\\ \Delta\beta\end{pmatrix} \tag{8}$$

where terms linear in $(\Delta\alpha,\Delta\beta)$ are 0 because the expansion is around the minimum of Q_{obs}, and

$$\mathbf{M} = \begin{pmatrix}\frac{\partial^2}{\partial\alpha^2} & \frac{\partial^2}{\partial\alpha\partial\beta}\\ \frac{\partial^2}{\partial\alpha\partial\beta} & \frac{\partial^2}{\partial\beta^2}\end{pmatrix} Q_{obs} = 2\begin{pmatrix}\overline{T_{hGHG}^2} & \overline{T_{hGHG}T_{haer}}\\ \overline{T_{hGHG}T_{haer}} & \overline{T_{haer}^2}\end{pmatrix} \tag{9}$$

The Hesse or curvature matrix $\mathbf{M}$ is characterized by its two positive eigenvalues λ_1 and λ_2 and associated eigenvectors $\mathbf{e_1}$ and $\mathbf{e_2}$, with $\lambda_1 < \lambda_2$. The extreme case of $T_{haer} \sim T_{hGHG}$, i.e. $\mathbf{M}$ is degenerate, would imply $\lambda_1 = 0$. This is not actually the case for any of the models considered here, but the two regressors are similar enough that λ_1 is close to 0. The analysis implies that the error function E_{obs} forms ellipses around the minimum with two orthogonal axes that point in the directions of the eigenvectors with curvatures in these directions proportional to $\sqrt{\lambda_1}$ and $\sqrt{\lambda_2}$.

I interpret the eigenvectors $\mathbf{e_1}$ and $\mathbf{e_2}$ as the directions in (α,β) parameter space that correspond to optimal cancellation (for $\mathbf{e_1}$) and optimal reinforcement (for $\mathbf{e_2}$) of the warming effects due to GHGs and aerosols. For the case of optimal cancellation, GHG warming and aerosol-induced cooling are at all statistically distinguishable in the observed temperature record because of a trend reversal in SO_2 precursor emissions in the late 20$^{\text{th}}$ century (Szopa et al., 2021) causing anthropogenic aerosol-induced cooling to be on a declining trend (in absolute terms) since then, in contrast to the monotonically increasing warming since 1850 associated with GHGs. This means that variations in the contributions of both processes in this direction of optimal cancellation cause detectable variations in the temperature trend of the final 20 years of the regression fit (2001-2020 or 1995-2014, respectively) that I will relate to the trend uncertainty of the observed temperature record. This analysis will define bounds E_{max} on the cost function E_{obs} and consequently the regression parameters (α_1,β_1). The analysis implies that regression parameters outside these bounds yield significantly and detectably inferior regression fits.

Variations in the direction of optimal reinforcement ($\mathbf{e_2}$) by contrast produce shifts of the regression fits away from the optimum in either direction. By comparing these shifts to the uncertainty in the mean of the detrended 2001-2020 (or 1995-2014, respectively) global temperature record (∼0.03 K in HadCRUT5) I find bounds on the cost function that are substantially more restrictive than the bounds associated with variations in the direction of optimal cancellation discussed above. I will

https://doi.org/10.5194/egusphere-2023-2427
Preprint. Discussion started: 18 December 2023

therefore only present an analysis to variations in the direction of cancellation $\mathbf{e_1}$ which yields more conservative, wider error bounds.

Analogously, I define an error function $E_{hist}(\alpha, \beta)$ for the regressions to the "historical" ensemble means:

$$E_{hist}(\alpha,\beta) \equiv \sqrt{\frac{\overline{r_{hist}^2(\alpha,\beta)}}{\overline{\epsilon_2^2}}}. \tag{10}$$

where

$$r_{hist}(\alpha,\beta) = T_{hist} - \alpha T_{GHG} - \beta T_{haer} - \gamma_2 T_{hnat}. \tag{11}$$

The ellipses spanned by E_{hist} have the same orientations and aspect ratios of the two main axes as those spanned by E_{obs}.

3 Evaluation

3.1 Example model calculations

As an example, figure 2 shows the result of the analysis for four models. GHGs drive a warming of around 2.1 K in the HadGEM3-GC31-LL model over 1850-2020 (light green line), offset by aerosol-driven cooling of around -0.9 K by 2020 (dark green). Natural influences explain the temporary features associated with volcanic eruptions and solar forcing (blue line). Optimal regression parameters α_2, β_2, and γ_2 for the "historical" simulation are close to 1 (i.e. HadGEM3-GC31-LL is nearly "additive", violet line). However, the regression against T_{obs} requires substantial reductions in the parameters describing both the GHG and the aerosol influences, to the point that the aerosol cooling would need to be reduced by around 85%, and the GHG influence by 40%, to match the observed record (orange line).

The other three models will be discussed in more detail below.

Figure A1 contains equivalent plots for the remaining 11 models.

3.1.1 When are two regression fits statistically indistinguishable?

I note that the observational record exhibits a nearly linear warming trend towards the end of the record (figure 2). Furthermore during much of the 20$^{\text{th}}$ century the aerosol-induced cooling is directly opposed to the GHG warming, but in the 1990s its trend changes sign in the HadGEM3-GC31-LL hist-aer ensemble. This trend reversal is a major reason that the GHG and aerosol influences are at all statistically distinguishable in the historical record. I thus define two regression fits to be significantly different if their 20-year trends for 2001-2020 (or 1995-2014, for CESM2, E3SM-2-0, and GISS-E2-1-G) differ by more than the observational uncertainties at 95% confidence in these trend ($\kappa = 6.7$ and 6.3 mK a^{-1}, respectively).

I evaluate the regression fits in regression parameter space (α, β) along the lines that correspond to optimal cancellation of the warming and cooling impacts of GHGs and aerosols, respectively. This is the line spanned by the eigenvector corresponding to the smaller eigenvalue λ_1, $\mathbf{e_1}$, i.e.

$$(\alpha,\beta) = (\alpha_1,\beta_1) + c \cdot \mathbf{e_1} \tag{12}$$

https://doi.org/10.5194/egusphere-2023-2427
Preprint. Discussion started: 18 December 2023

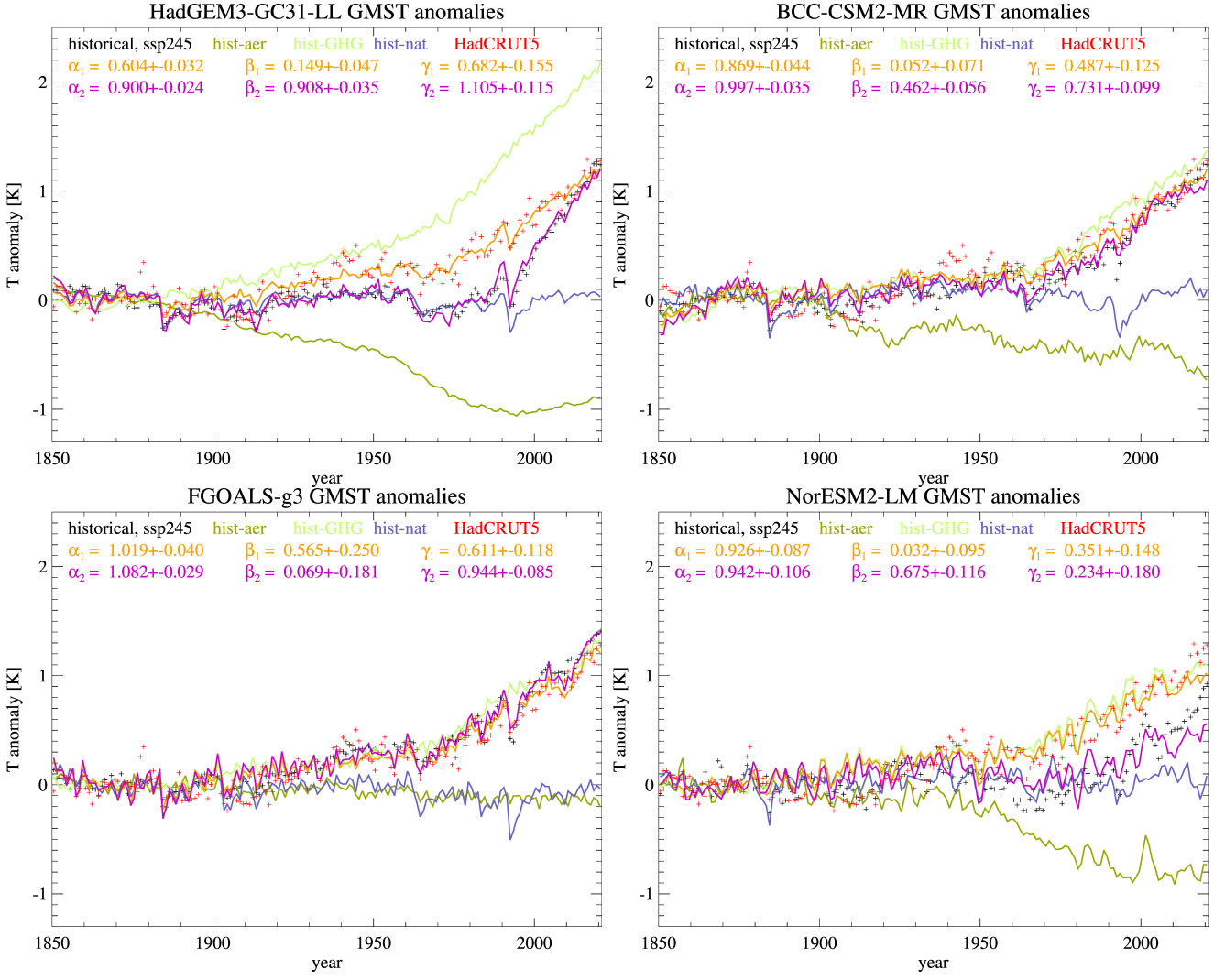

Figure 2. Ensemble-, global-, and annual-mean temperature anomalies relative to the 1850-1899 average for HadGEM3-GC31-LL, BCC-CSM2-MR, FGOALS-g3, and NorESM2-LM. Black symbols and dark green, light green, and blue lines: The DAMIP and "historical" ensemble means as indicated. Violet: Optimal regression fits to T_{hist} following equation 2. Orange: Optimal regression fits to T_{obs}, the HadCRUT5 reconstruction, following equation 1. Red symbols: HadCRUT5 (Morice et al., 2021). The regression coefficients α_1, β_1, γ_1, α_2, β_2, and γ_2 that are stated in orange and violet are as defined in equations 1 and 2.

This line marks the direction of maximum joint uncertainty in the regression parameters.

I plot the error functions E_{obs} against the 2001-2020 (or 1995-2014) trends in the associated fits $T(\alpha,\beta) = \alpha T_{hGHG} + \beta T_{haer} + \gamma_1 T_{nat}$, evaluated along the line described by eq. 12 (figure 3). By evaluating E_{obs} at the two trend values that differ from the trend in the optimal solution by κ, I find model-dependent values for E_{max}. For all but three of the models $E_{max} \leq 1.14$. However, BCC-CSM2-LR, FGOALS-g3, and NorESM2-LM have anomalously large such thresholds. These

https://doi.org/10.5194/egusphere-2023-2427
Preprint. Discussion started: 18 December 2023

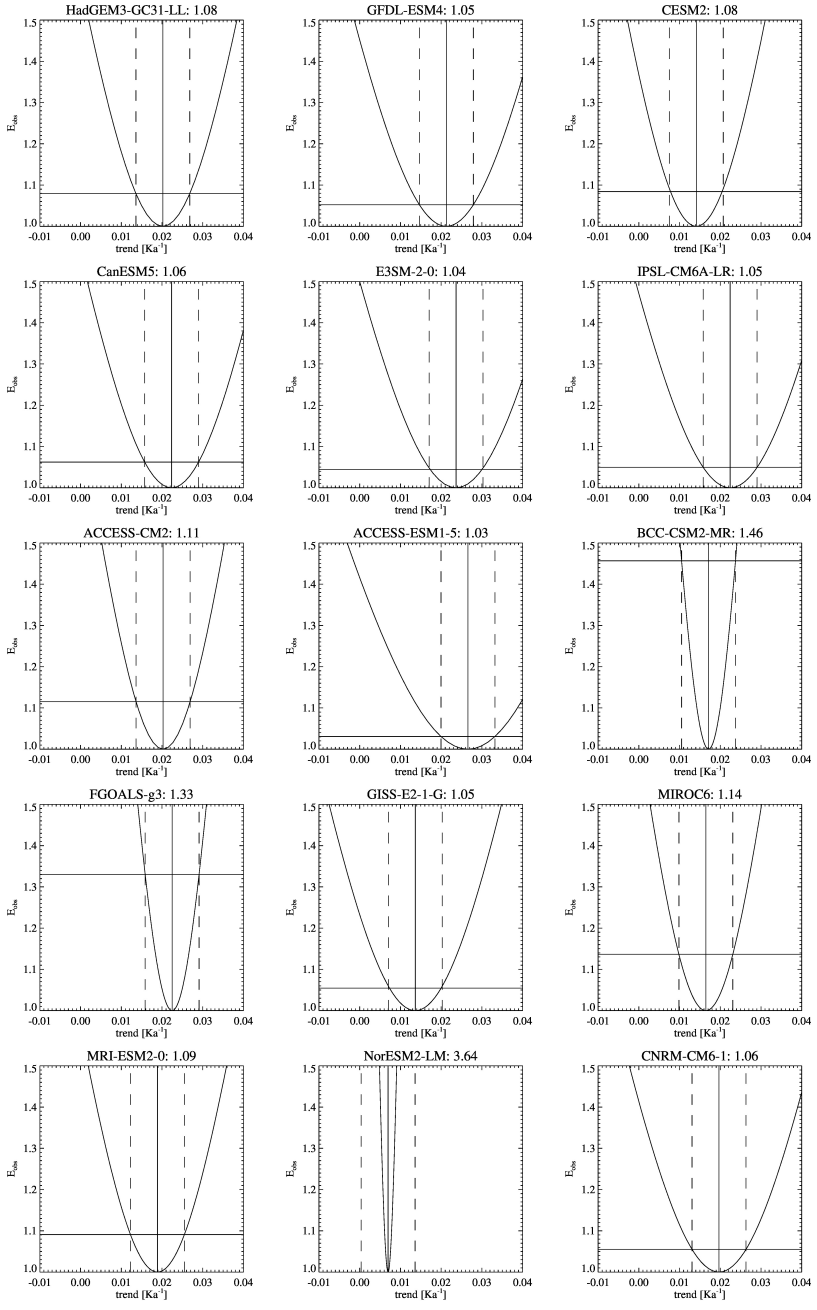

Figure 3. Error function E_{obs} as a function of the 2001-2020 (for CESM2, E3SM-2-0, and GISS-E2-1-G: 1995-2014) temperature trends in the regression fits to T_{obs} (eq. 1), for the DAMIP models. The trends are evaluated along the line in (α, β) parameter space described by equation 12. Vertical solid line: Trend in the optimal fit (that minimizes E_{obs}). Vertical dashed lines: Trends in the sub-optimal fits that differ from the optimal trend by the observational trend uncertainty κ. Horizontal line: Value of the error function corresponding to this trend uncertainty. The number in the titles is the value of the error function at these points.

https://doi.org/10.5194/egusphere-2023-2427
Preprint. Discussion started: 18 December 2023

models' simulations of tas are displayed in figure 2. NorESM2-LM simulates a large warming spike around 2002 in its hist-aer ensemble-mean temperature timeseries, giving an anomalous cooling trend for 2001-2020. FGOALS-g3 produces almost no cooling in its hist-aer ensemble. BCC-CSM2-LR exhibts continuing cooling in its hist-aer ensemble in this period, with an anomalous, warm spell in the 2010s. In these three cases, the threshold of detectability, reliant on a significant change in the overall cooling trend in the hist-aer ensemble at the end of this experiment, does not work well. The other 12 models yielding smaller, regular values for E_{max} all simulate a substantial change in the rate of cooling such that their hist-aer temperature timeseries become statistically independent from their hist-GHG temperatures, and almost all exhibit warming trends during the final two decades of their hist-aer ensembles (figures 2 and A1).

3.2 Joint uncertainty analysis of the GHG and aerosol influences for all models

Figure 4 illustrates firstly that additivity does not extend to all models, i.e. $(\alpha, \beta) = (1, 1)$ is well outside the contoured uncertainty ellipses of the T_{hist} regressions for most models.

In all cases except for two of the anomalous models (BCC-CSM2-MR, FGOALS-g3) there are no overlaps between the regression uncertainty ellipses for the fits to T_{obs} and T_{hist}. This means 13 of the models have systematic differences between the simulated historical and the observed temperature evolutions large enough to show in this lack of overlap of the regression parameters. This implies irreconcilable scaling factors α and β for the GHG or aerosol influences, or both.

Specifically regarding the GHG rescaling factor α (plotted on the vertical axes in figure 4), for some large-ECS models including ACCESS-CM2, CanESM5, CESM2, HadGEM3-GC31-LL, and IPSL-CM6-LR, the analysis suggests that $\alpha_2 < \alpha_1$ or $A < 1$, i.e. to better match the HadCRUT5 timeseries, the GHG influences in these models need to be scaled down.

Lastly, for almost all models the analysis suggests that the aerosol rescaling factor β_1 derived from T_{obs} is smaller than β_2 derived from T_{hist} (i.e., in figure 4 the coloured ellipses are to the left of the contoured ellipses). Exceptions are the FGOALS-g3 model (discussed above) and the IPSL-CM6A-LR and MIROC6 models where both regressions yield about the same aerosol influence. Exaggeration of the aerosol influence is particularly large and unambiguous for ACCESS-CM2, ACCESS-ESM1-5, CanESM5, E3SM-2-0, HadGEM3-GC31, and NorESM2-LM; these models all simulate at least -0.7K of cooling in their hist-aer ensembles.

3.3 Emergent constraints for the ECS and the aerosol cooling influence

3.3.1 The GHG influence

Figure 5 shows the result of the regression analysis (section 2.2) for all models. The ensemble includes three models (CanESM5, CESM2, HadGEM3-GC31-LL) that have ECSs outside the very likely range given by AR6 (2 to 5 K, Forster et al., 2021, figure 5a). For these three models, the GHG correction factor $A < 1$ (i.e. a reduction of the GHG influence would bring their historical simulations into better agreement with the observations). Particularly for CanESM5, with an ECS of 5.6K, this reduction is quite large, amounting to a 50% reduction of the GHG induced warming. At the other end of the spectrum, MIROC6, with an ECS of 2.6 K, requires an increase in the GHG-induced warming by 33% to bring its historical evolution into agreement

https://doi.org/10.5194/egusphere-2023-2427
Preprint. Discussion started: 18 December 2023

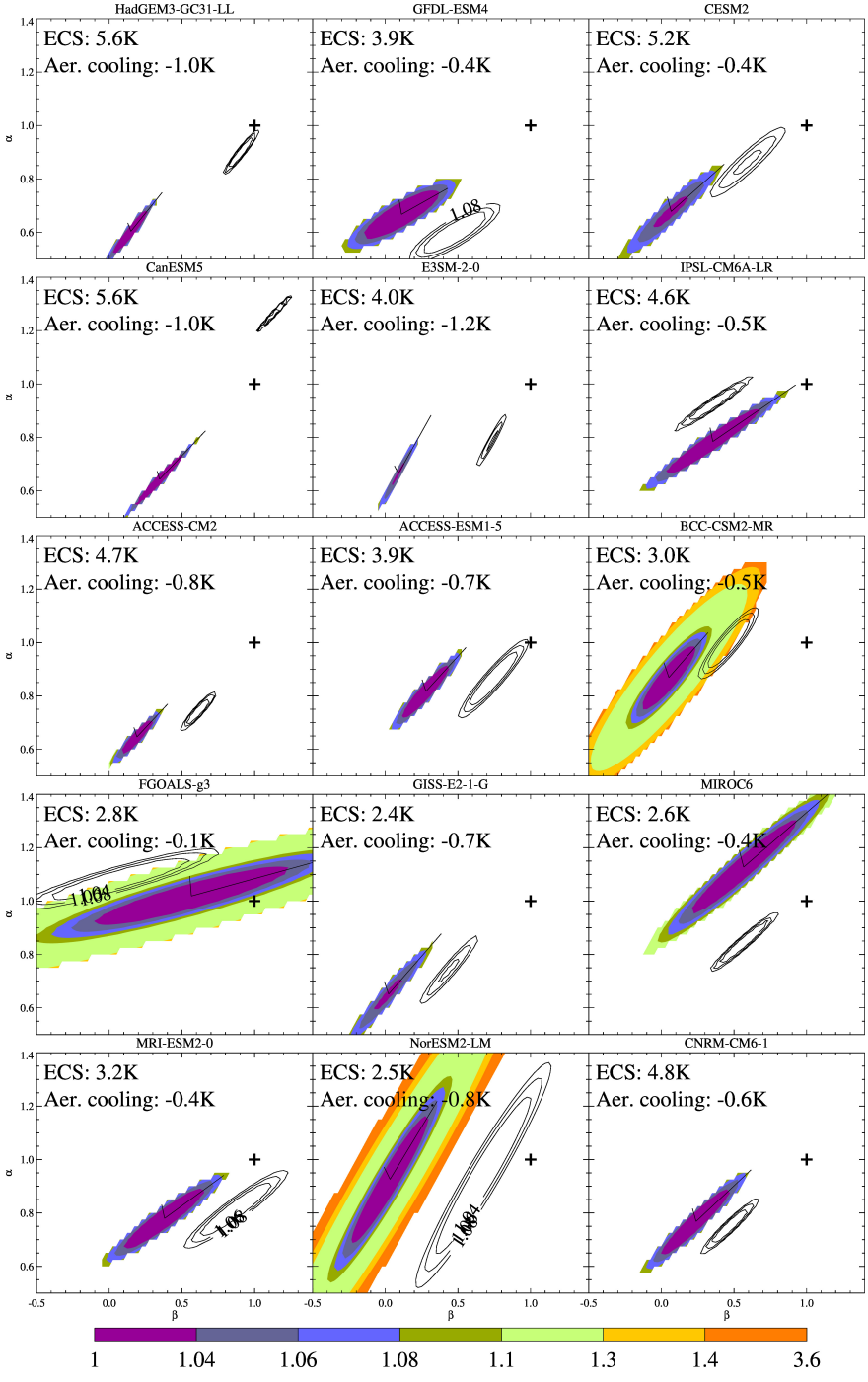

Figure 4. Error functions E_{obs} (colours, eq. 7) and E_{hist} (contours, eq. 10) where these functions are smaller than $\max(E_{max}, 1.1)$, for the 15 DAMIP models. '+' symbol: $\alpha = \beta = 1$. "Aer. cooling" is the global-, ensemble-, and annual-mean cooling for 2000-2014 relative to 1850-1899 as simulated in the models' hist-aer ensembles. "ECS" is as in table 1.

https://doi.org/10.5194/egusphere-2023-2427
Preprint. Discussion started: 18 December 2023

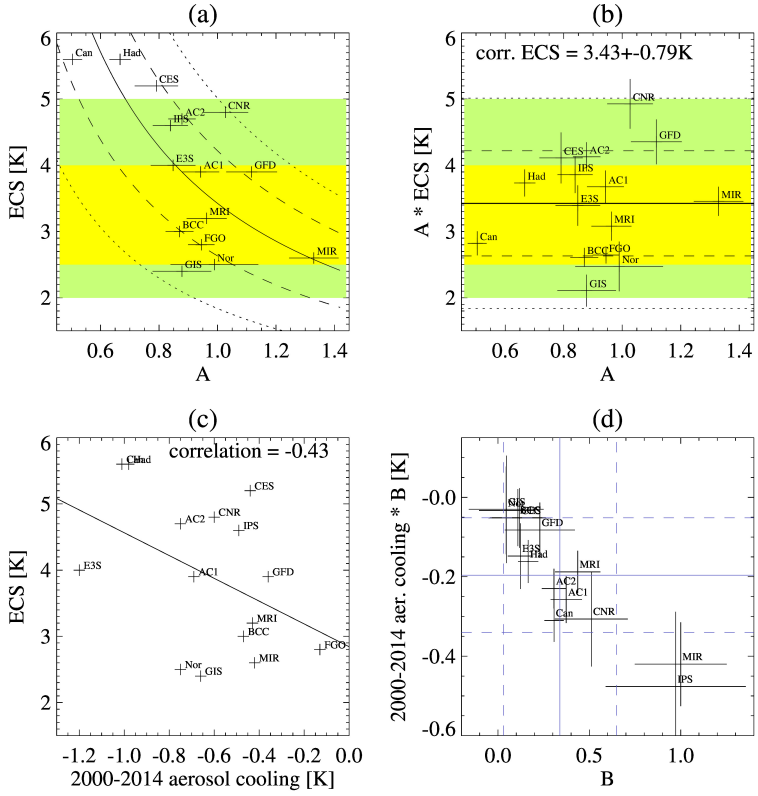

Figure 5. (a) The models' ECSs (K) versus A (equation 3). The lengths of the horizontal lines depict the regression uncertainties at 68% confidence. Solid line: Regression fit assuming ECS$\cdot A$ = const. Dashed and dotted lines: Uncertainty ranges at 68 and 95% confidence. The yellow and green regions are the likely (i.e. 66% confidence) and very likely (90%) ECS intervals (Forster et al., 2021). (b) Same as (a) but for ECS$\cdot A$ versus A. The solid, dashed and dotted lines are the mean and the 68 and 95% confidence intervals. (c) The tabulated ECSs versus cooling simulated in the hist-aer ensembles for 2000-2014 relative to 1850-1899. Solid fit: Best linear fit. (d) The aerosol-induced cooling taken from hist-aer times B (K) versus the correction factors to aerosol cooling B (equation 3). Solid and dashed lines denote the means and 68% confidence limits of both quantities.

with HadCRUT5. In general, the distribution (panel a) can be approximated by ECS $\sim A^{-1}$. Equivalently, panel (b) shows the ECS $\cdot A$ versus A. The thus "adjusted" ECSs (i.e., ECS $\cdot A$) are now within the AR6 "very likely" range for all models, and the multi-model spread is similar to the AR6 uncertainty range. We obtain a multi-model-mean adjusted ECS of 3.4 ± 0.8 K at 68% confidence (figure 5b).

https://doi.org/10.5194/egusphere-2023-2427
Preprint. Discussion started: 18 December 2023

3.3.2 The aerosol influence

The second part of this analysis concerns the aerosol-induced cooling. There is an anticorrelation (with a correlation coefficient of -0.43) between the cooling attributable to anthropogenic aerosol increases, as discerned from hist-aer, and the ECSs of the 15 models (figure 5c). This means that large-ECS models tend to compensate some of their GHG-induced warming by simulating a relatively large cooling due to aerosols. In other words, the biases in both properties are coupled.

As noted above, 12 of the 15 models require substantial decreases of the aerosol-induced cooling (i.e. $B \leq 0.5$) to bring their simulations into optimal agreement with HadCRUT5. Only one model (FGOALS-g3) requires a substantial ($B = 8$) increase in this cooling. This model simulates an anomalously small aerosol-related cooling of only around -0.1 K in its hist-aer ensemble (figure 5c), and I derive a highly anomalous regression coefficient of $\beta_2 = 0.07$ to bring the hist-aer simulated cooling into agreement with the historical ensemble by this model. For this reason the model is not considered in the aerosol part of the analysis conducted here. For MIROC6 and IPSL-CM6A-LR, the correction $B \approx 1$, i.e. these models simulate the optimal magnitude of aerosol-induced cooling. Seven of the remaining 12 models have $0 < B < 0.25$, i.e. the aerosol-induced cooling would need to reduce by more than 3/4. This group includes some models with large aerosol-induced cooling such as HadGEM3-GC31-LL, NorESM2, and E3SM-2-0. The corrected aerosol-induced cooling averages to -0.19 ± 0.14K between 1850-1899 and 2000-2014 and the average scaling factor B is 0.34$\pm$0.31, i.e. as a group the analysis implies that a 2/3 reduction in aerosol-related cooling would bring the models into agreement with the HadCRUT5 climatology. The 14-model average actual simulated cooling is -0.63 ± 0.28K.

4 Conclusions and discussion

Mismatches between the observed global-mean surface temperature and CMIP6 “historical" simulated temperature have been documented before and attributed, in some cases, to a deficient simulation of aerosol-related cooling (Andrews et al., 2020; Flynn and Mauritsen, 2020; Smith and Forster, 2021; Golaz et al., 2022). Here I exploit these mismatches to derive scaling factors for the GHG-induced warming and the aerosol-related cooling on temperature that in a hypothetical model would bring the simulated historical temperature into optimal agreement with the HadCRUT5 climatology. I then relate these scaling factors to the warming attributable to GHGs, on the one hand, and on the other hand to the cooling attributable to anthropogenic aerosols. The GHG scaling factors very approximately follow an inverse relationship with the ECSs of the models, such that the products of the ECSs and the scaling factors are in better agreement with the AR6 evaluation of the planetary ECS than the modelled ECSs themselves. Particularly, for three large-ECS models with ECSs outside the AR6 “very likely" range (Forster et al., 2021), this adjustment brings these ECSs into agreement with the AR6 estimate. However, the multi-model disagreement in the scaled ECSs still remains considerable.

These results are consistent with Smith and Forster (2021) but arrived at using an independent approach. Smith and Forster (2021) use energy budget constraints to find that despite reductions in historical aerosol and GHG forcing from CMIP5 to CMIP6, stronger climate feedbacks in CMIP6 models, which are reflected in the increased ECSs in CMIP6 models, cause both stronger aerosol cooling and from 1990 increased GHG warming. This analysis generally confirms their results and but shows

https://doi.org/10.5194/egusphere-2023-2427
Preprint. Discussion started: 18 December 2023

that the overestimation of aerosol-induced cooling pertains not just to the high-ECS models but to many of the moderate-ECS models as well. Only three models do not exhibit this behaviour, characterized by both high (IPSL-CM6A-LR) and moderate (MIROC6, FGOALS-g3) ECSs.

I find an anticorrelation between the total simulated aerosol-induced cooling since 1850 and the ECSs of the models, suggesting that both quantities are coupled and that there could be a compensation of errors between these two processes. 12 out of 15 models exhibit aerosol cooling scaling factors smaller than 0.5 to optimally reconcile their aerosol-related cooling with the historical record. The result suggests that the large majority of DAMIP models considerably overestimates aerosol-induced cooling. Using 14 models with aerosol scaling factors between 0 and 1.1, we derive an average correction factor for the aerosol-induced cooling of 0.34 ± 0.31 and a mean cooling by 2000-2014, relative to 1850-1899, of -0.19 ± 0.14K (both at 68% confidence). This means some stronger simulated aerosol-induced cooling, exceeding -0.5K in the cases of eight models, is very likely unrealistic.

There are two limitations to the analysis presented here: The first is that the hist-GHG experiment quantifies the responses of the climate models to all GHGs in combination, whereas the ECSs are an expression of the sensitivity of climate only to CO_2 increases. I have shown that there is a near-perfect proportionality and a high degree of correlation (0.78) between the warmings simulated in hist-GHG and the ECSs in the 15 models used here (figure 1), suggesting that the substantial model diversities that exist for both quantities are due to the same processes, i.e. climate feedbacks e.g. due to cloud adjustments that are not sensitive to the detailed properties of the driving GHGs.

The other, more fundamental limitation is that the models do not respond perfectly additively to GHG and aerosol forcing. This is expressed in deviations from 1 for the α_2, β_2, and γ_2 parameters in equation 2 (figure 4). The non-additivity could be due to a variety of reasons, including forcings not included in the analysis (such as land use changes and ozone changes). Whilst these are usually considered relatively small forcers on the global scale (Forster et al., 2021), I have tested the sensitivity of the results to including, in equations 1 and 2, terms for the temperature anomalies simulated under the hist-totalO3 experiment in which all forcings except ozone are held constant. Three models (CanESM5, GISS-E2-1-G, and MIROC6) have completed this experiment. Ozone changes are the most important anthropogenic radiative forcing agent after those considered here (GHGs and aerosols, Forster et al., 2021). However, expanding the regression model in this way produces only minimal differences for the regression coefficients in the cases of those three models (not shown), suggesting that my regression model is set up correctly, covering the attributable global drivers of climate change for tas.

For the aerosol influence, for several models we deduce aerosol regression coefficients $\beta_2 < 0.5$ (equation 2), namely BCC-CSM2-MR, CNRM-CM6-1, GFDL-ESM4, GISS-E2-1-G, IPSL-CM6A-LR, and FGOALS-g3. Such large deviations from unity call into question the suitability of these models' hist-aer simulations for attribution. However, several other models indicating that large reductions in aerosol cooling would be beneficial for bringing the simulated historical temperature record into better agreement with observations, including ACCESS-ESM1-5, CanESM5, E3SM-2-0, HadGEM3-GC31-LL, and, MRI-ESM2-0, all have $\beta_2 > 0.7$, i.e. these models behave relatively additively, and the inference that exaggerated historical aerosol-induced cooling contributes substantially to errors in the simulations of global-mean tas by these models is quite well founded.

https://doi.org/10.5194/egusphere-2023-2427
Preprint. Discussion started: 18 December 2023

In summary, I have used a reconstruction of global-mean surface temperature and DAMIP and historical simulations by 15 contemporary climate models to derive constraints for the GHG-induced warming and the aerosol-induced cooling, by far the leading influences driving global warming. Using an emergent constraint approach, I derive a "corrected" ensemble-mean equilibrium climate sensitivity of about 3.4±0.8 K (at 68% confidence), in excellent agreement with the AR6 estimate (Forster et al., 2021). More importantly, I find that for 12 of these models, substantial reductions in the aerosol-induced cooling, along with some reductions in the GHG-induced warming for models with large ECSs, would bring their historical simulations into better agreement with the observational record. The results presented here highlight ongoing difficulties with correctly representing climate feedbacks in global models. Substantial, systematic, and nearly community-wide issues with representing historical global surface temperature reduce confidence in quantitative projections of global warming by models affected by these problems. Interestingly, at least some CMIP3 models were consistent with observations without any need for rescaling the aerosol and GHG signatures (Stone et al., 2007b), including for the precursor of CESM2 (Stone et al., 2007a). This suggests that at least for this model development occurring in the intervening time has introduced this problem.

The analysis is limited by the substantial anticorrelation between the GHG and the aerosol global-mean warming signatures. I anticipate that as anthropogenic aerosol production continues, as projected, to decline in the future (Lee et al., 2021), the anti-correlation between GHG-induced warming and aerosol-induced cooling will reduce, allowing for a more confident attribution of their respective roles in driving global warming.

Data availability. All model data used here have been downloaded from the Earth System Grid Federation, e.g. https://esgf-node.llnl.gov/search/cmip6/. HadCRUT5.0.1.0 data were obtained from http://www.metoffice.gov.uk/hadobs/hadcrut5 on 1 July 2023 and are © British Crown Copyright, Met Office [2019], provided under an Open Government License, http://www.nationalarchives.gov.uk/doc/open-government-licence/version/3/.

Appendix A: Regression fits for the remaining models

For models not represented in figure 2, the regression fits are given below.

A1

Author contributions. OM conceived of and conducted the analysis and wrote the paper.

Competing interests. The author declares no competing interests.

https://doi.org/10.5194/egusphere-2023-2427
Preprint. Discussion started: 18 December 2023

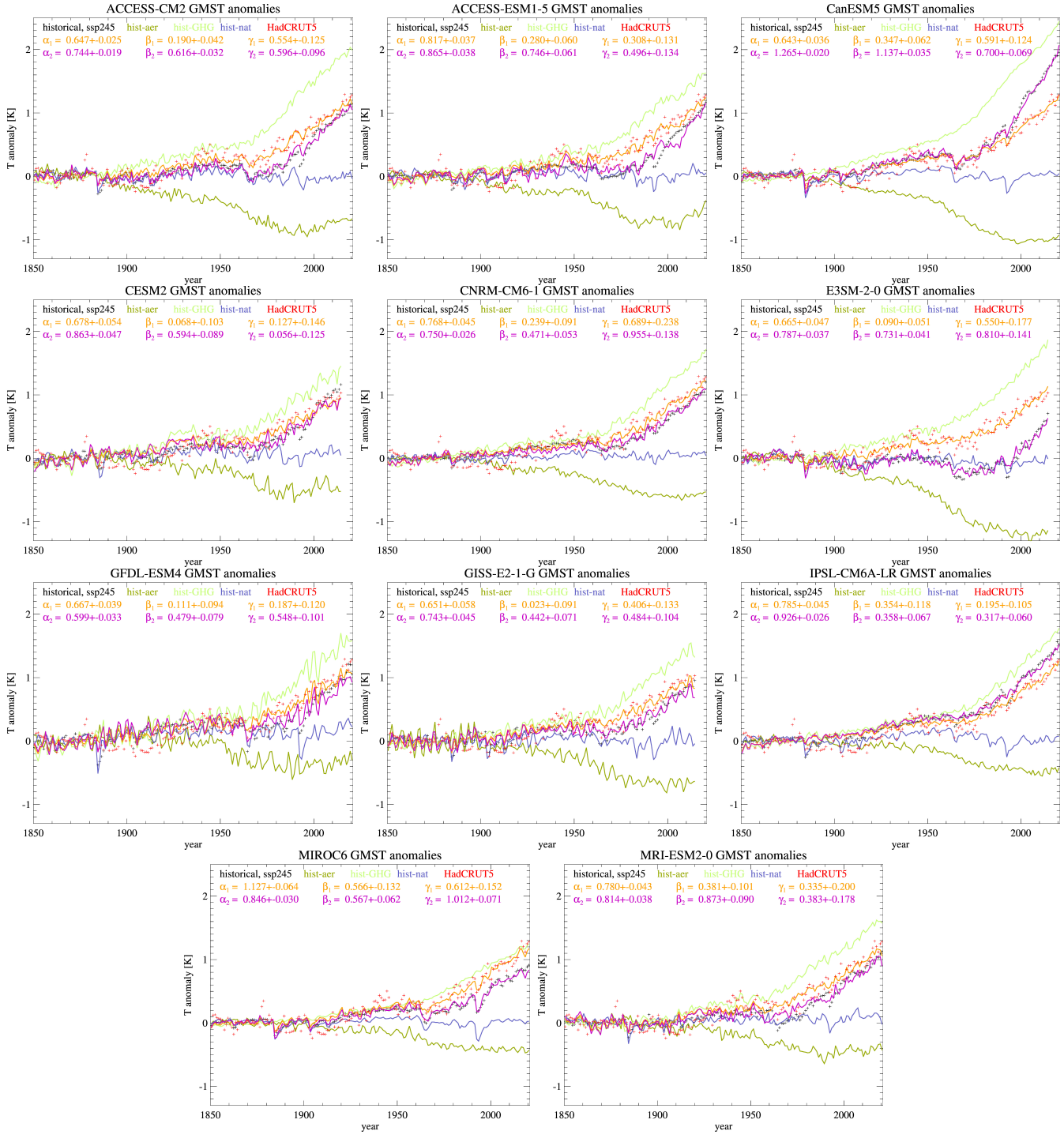

Figure A1. Same as figure 2 but for the ACCESS-CM2, ACCESS-ESM1-5, CanESM5, CESM2, CNRM-CM6-1, E3SM-2-0, GFDL-ESM4, GISS-E2-1-G, IPSL-CM6A-LR, MIROC6, and MRI-ESM2-0 models.

https://doi.org/10.5194/egusphere-2023-2427
Preprint. Discussion started: 18 December 2023

Acknowledgements. I acknowledge fruitful discussions with Dáithí Stone. I acknowledge the World Climate Research Programme, which, through its Working Group on Coupled Modelling, coordinated and promoted CMIP6. I thank the climate modeling groups for producing and making available their model output, the Earth System Grid Federation (ESGF) for archiving the data and providing access, and the multiple funding agencies who support CMIP6 and ESGF. I acknowledge the UK MetOffice for providing the HadCRUT5 data.

https://doi.org/10.5194/egusphere-2023-2427
Preprint. Discussion started: 18 December 2023

References

Andreae, M., Jones, C., and Cox, P.: Strong present-day aerosol cooling implies a hot future, Nature, 435, 1187–1190, https://doi.org/10.1038/nature03671, 2005.

Andrews, M. B., Ridley, J. K., Wood, R. A., Andrews, T., Blockley, E. W., Booth, B., Burke, E., Dittus, A. J., Florek, P., Gray, L. J., Haddad, S., Hardiman, S. C., Hermanson, L., Hodson, D., Hogan, E., Jones, G. S., Knight, J. R., Kuhlbrodt, T., Misios, S., Mizielinski, M. S., Ringer, M. A., Robson, J., and Sutton, R. T.: Historical simulations with HadGEM3-GC3.1 for CMIP6, Journal of Advances in Modeling Earth Systems, 12, e2019MS001 995, https://doi.org/https://doi.org/10.1029/2019MS001995, e2019MS001995 10.1029/2019MS001995, 2020.

Arrhenius, S.: Nature's heat usage, Nord. Tidsk., pp. 121–130, 1896.

Boucher, O., Denvil, S., Levavasseur, G., Cozic, A., Caubel, A., Foujols, M.-A., Meurdesoif, Y., Cadule, P., Devilliers, M., Ghattas, J., Lebas, N., Lurton, T., Mellul, L., Musat, I., Mignot, J., and Cheruy, F.: IPSL IPSL-CM6A-LR model output prepared for CMIP6 CMIP historical, https://doi.org/10.22033/ESGF/CMIP6.5195, 2018a.

Boucher, O., Denvil, S., Levavasseur, G., Cozic, A., Caubel, A., Foujols, M.-A., Meurdesoif, Y., and Gastineau, G.: IPSL IPSL-CM6A-LR model output prepared for CMIP6 DAMIP hist-GHG, https://doi.org/10.22033/ESGF/CMIP6.13825, 2018b.

Boucher, O., Denvil, S., Levavasseur, G., Cozic, A., Caubel, A., Foujols, M.-A., Meurdesoif, Y., and Gastineau, G.: IPSL IPSL-CM6A-LR model output prepared for CMIP6 DAMIP hist-aer, https://doi.org/10.22033/ESGF/CMIP6.13827, 2018c.

Boucher, O., Denvil, S., Levavasseur, G., Cozic, A., Caubel, A., Foujols, M.-A., Meurdesoif, Y., and Gastineau, G.: IPSL IPSL-CM6A-LR model output prepared for CMIP6 DAMIP hist-nat, https://doi.org/10.22033/ESGF/CMIP6.13831, 2018d.

Boucher, O., Denvil, S., Levavasseur, G., Cozic, A., Caubel, A., Foujols, M.-A., Meurdesoif, Y., Cadule, P., Devilliers, M., Dupont, E., and Lurton, T.: IPSL IPSL-CM6A-LR model output prepared for CMIP6 ScenarioMIP ssp245, https://doi.org/10.22033/ESGF/CMIP6.5264, 2019.

Danabasoglu, G.: NCAR CESM2 model output prepared for CMIP6 CMIP historical, https://doi.org/10.22033/ESGF/CMIP6.7627, 2019a.

Danabasoglu, G.: NCAR CESM2 model output prepared for CMIP6 DAMIP hist-GHG, https://doi.org/10.22033/ESGF/CMIP6.7604, 2019b.

Danabasoglu, G.: NCAR CESM2 model output prepared for CMIP6 DAMIP hist-nat, https://doi.org/10.22033/ESGF/CMIP6.7609, 2019c.

Danabasoglu, G.: NCAR CESM2 model output prepared for CMIP6 DAMIP hist-aer, https://doi.org/10.22033/ESGF/CMIP6.7605, 2020.

Dix, M., Bi, D., Dobrohotoff, P., Fiedler, R., Harman, I., Law, R., Mackallah, C., Marsland, S., O'Farrell, S., Rashid, H., Srbinovsky, J., Sullivan, A., Trenham, C., Vohralik, P., Watterson, I., Williams, G., Woodhouse, M., Bodman, R., Dias, F. B., Domingues, C. M., Hannah, N., Heerdegen, A., Savita, A., Wales, S., Allen, C., Druken, K., Evans, B., Richards, C., Ridzwan, S. M., Roberts, D., Smillie, J., Snow, K., Ward, M., and Yang, R.: CSIRO-ARCCSS ACCESS-CM2 model output prepared for CMIP6 CMIP historical, https://doi.org/10.22033/ESGF/CMIP6.4271, 2019a.

Dix, M., Bi, D., Dobrohotoff, P., Fiedler, R., Harman, I., Law, R., Mackallah, C., Marsland, S., O'Farrell, S., Rashid, H., Srbinovsky, J., Sullivan, A., Trenham, C., Vohralik, P., Watterson, I., Williams, G., Woodhouse, M., Bodman, R., Dias, F. B., Domingues, C. M., Hannah, N., Heerdegen, A., Savita, A., Wales, S., Allen, C., Druken, K., Evans, B., Richards, C., Ridzwan, S. M., Roberts, D., Smillie, J., Snow, K., Ward, M., and Yang, R.: CSIRO-ARCCSS ACCESS-CM2 model output prepared for CMIP6 ScenarioMIP ssp245, https://doi.org/10.22033/ESGF/CMIP6.4321, 2019b.

Dix, M., Mackallah, C., Bi, D., Bodman, R., Marsland, S., Rashid, H., Woodhouse, M., and Druken, K.: CSIRO-ARCCSS ACCESS-CM2 model output prepared for CMIP6 DAMIP hist-GHG, https://doi.org/10.22033/ESGF/CMIP6.14365, 2020a.

https://doi.org/10.5194/egusphere-2023-2427
Preprint. Discussion started: 18 December 2023

Dix, M., Mackallah, C., Bi, D., Bodman, R., Marsland, S., Rashid, H., Woodhouse, M., and Druken, K.: CSIRO-ARCCSS ACCESS-CM2 model output prepared for CMIP6 DAMIP hist-aer, https://doi.org/10.22033/ESGF/CMIP6.14369, 2020b.

Dix, M., Mackallah, C., Bi, D., Bodman, R., Marsland, S., Rashid, H., Woodhouse, M., and Druken, K.: CSIRO-ARCCSS ACCESS-CM2 model output prepared for CMIP6 DAMIP hist-nat, https://doi.org/10.22033/ESGF/CMIP6.14377, 2020c.

E3SM: E3SM-Project E3SM2.0 model output prepared for CMIP6 CMIP historical, http://cera-www.dkrz.de/WDCC/meta/CMIP6/CMIP6.CMIP.E3SM-Project.E3SM-2-0.historical, 2022a.

E3SM: E3SM-Project E3SM2.0 model output prepared for CMIP6 DAMIP hist-GHG, http://cera-www.dkrz.de/WDCC/meta/CMIP6/CMIP6.DAMIP.E3SM-Project.E3SM-2-0.hist-GHG, 2022b.

E3SM: E3SM-Project E3SM2.0 model output prepared for CMIP6 DAMIP hist-aer, http://cera-www.dkrz.de/WDCC/meta/CMIP6/CMIP6.DAMIP.E3SM-Project.E3SM-2-0.hist-aer, 2022c.

E3SM: E3SM-Project E3SM2.0 model output prepared for CMIP6 DAMIP hist-nat, http://cera-www.dkrz.de/WDCC/meta/CMIP6/CMIP6.DAMIP.E3SM-Project.E3SM-2-0.hist-nat, 2022d.

Eyring, V., Bony, S., Meehl, G. A., Senior, C. A., Stevens, B., Stouffer, R. J., and Taylor, K. E.: Overview of the Coupled Model Intercomparison Project Phase 6 (CMIP6) experimental design and organization, Geoscientific Model Development, 9, 1937–1958, https://doi.org/10.5194/gmd-9-1937-2016, 2016.

Flynn, C. M. and Mauritsen, T.: On the climate sensitivity and historical warming evolution in recent coupled model ensembles, Atmospheric Chemistry and Physics, 20, 7829–7842, https://doi.org/10.5194/acp-20-7829-2020, 2020.

Forster, P., Storelvmo, T., Armour, K., Collins, W., Dufresne, J.-L., Frame, D., Lunt, D., Mauritsen, T., Palmer, M., Watanabe, M., Wild, M., and Zhang, H.: The Earth's Energy Budget, Climate Feedbacks, and Climate Sensitivity, in: Climate Change 2021: The Physical Science Basis. Contribution of Working Group I to the Sixth Assessment Report of the Intergovernmental Panel on Climate Change, edited by Masson-Delmotte, V., Zhai, P., Pirani, A., Connors, S., Péan, C., Berger, S., Caud, N., Chen, Y., Goldfarb, L., Gomis, M., Huang, M., Leitzell, K., Lonnoy, E., Matthews, J., Maycock, T., Waterfield, T., Yelekçi, O., Yu, R., and Zhou, B., p. 923–1054, Cambridge University Press, Cambridge, United Kingdom and New York, NY, USA, https://doi.org/10.1017/9781009157896.009, 2021.

Gidden, M. J., Riahi, K., Smith, S. J., Fujimori, S., Luderer, G., Kriegler, E., van Vuuren, D. P., van den Berg, M., Feng, L., Klein, D., Calvin, K., Doelman, J. C., Frank, S., Fricko, O., Harmsen, M., Hasegawa, T., Havlik, P., Hilaire, J., Hoesly, R., Horing, J., Popp, A., Stehfest, E., and Takahashi, K.: Global emissions pathways under different socioeconomic scenarios for use in CMIP6: a dataset of harmonized emissions trajectories through the end of the century, Geoscientific Model Development, 12, 1443–1475, https://doi.org/10.5194/gmd-12-1443-2019, 2019.

Gillett, N. P., Shiogama, H., Funke, B., Hegerl, G., Knutti, R., Matthes, K., Santer, B. D., Stone, D., and Tebaldi, C.: The Detection and Attribution Model Intercomparison Project (DAMIP v1.0) contribution to CMIP6, Geoscientific Model Development, 9, 3685–3697, https://doi.org/10.5194/gmd-9-3685-2016, 2016.

Golaz, J.-C., Van Roekel, L. P., Zheng, X., Roberts, A. F., Wolfe, J. D., Lin, W., Bradley, A. M., Tang, Q., Maltrud, M. E., Forsyth, R. M., Zhang, C., Zhou, T., Zhang, K., Zender, C. S., Wu, M., Wang, H., Turner, A. K., Singh, B., Richter, J. H., Qin, Y., Petersen, M. R., Mametjanov, A., Ma, P.-L., Larson, V. E., Krishna, J., Keen, N. D., Jeffery, N., Hunke, E. C., Hannah, W. M., Guba, O., Griffin, B. M., Feng, Y., Engwirda, D., Di Vittorio, A. V., Dang, C., Conlon, L. M., Chen, C.-C.-J., Brunke, M. A., Bisht, G., Benedict, J. J., Asay-Davis, X. S., Zhang, Y., Zhang, M., Zeng, X., Xie, S., Wolfram, P. J., Vo, T., Veneziani, M., Tesfa, T. K., Sreepathi, S., Salinger, A. G., Reeves Eyre, J. E. J., Prather, M. J., Mahajan, S., Li, Q., Jones, P. W., Jacob, R. L., Huebler, G. W., Huang, X., Hillman, B. R., Harrop, B. E., Foucar, J. G., Fang, Y., Comeau, D. S., Caldwell, P. M., Bartoletti, T., Balaguru, K., Taylor, M. A., McCoy, R. B., Leung, L. R., and Bader,

https://doi.org/10.5194/egusphere-2023-2427
Preprint. Discussion started: 18 December 2023

D. C.: The DOE E3SM model Vversion 2: Overview of the physical model and initial model evaluation, Journal of Advances in Modeling Earth Systems, 14, e2022MS003 156, https://doi.org/https://doi.org/10.1029/2022MS003156, e2022MS003156 2022MS003156, 2022.

Good, P.: MOHC HadGEM3-GC31-LL model output prepared for CMIP6 ScenarioMIP ssp245, https://doi.org/10.22033/ESGF/CMIP6.10851, 2019.

Horowitz, L. W., John, J. G., Blanton, C., McHugh, C., Radhakrishnan, A., Rand, K., Vahlenkamp, H., Zadeh, N. T., Wilson, C., Dunne, J. P., Ploshay, J., Winton, M., and Zeng, Y.: NOAA-GFDL GFDL-ESM4 model output prepared for CMIP6 DAMIP hist-GHG, https://doi.org/10.22033/ESGF/CMIP6.8570, 2018a.

Horowitz, L. W., John, J. G., Blanton, C., McHugh, C., Radhakrishnan, A., Rand, K., Vahlenkamp, H., Zadeh, N. T., Wilson, C., Dunne, J. P., Ploshay, J., Winton, M., and Zeng, Y.: NOAA-GFDL GFDL-ESM4 model output prepared for CMIP6 DAMIP hist-aer, https://doi.org/10.22033/ESGF/CMIP6.8571, 2018b.

Horowitz, L. W., John, J. G., Blanton, C., McHugh, C., Radhakrishnan, A., Rand, K., Vahlenkamp, H., Zadeh, N. T., Wilson, C., Dunne, J. P., Ploshay, J., Winton, M., and Zeng, Y.: NOAA-GFDL GFDL-ESM4 model output prepared for CMIP6 DAMIP hist-nat, https://doi.org/10.22033/ESGF/CMIP6.8575, 2018c.

John, J. G., Blanton, C., McHugh, C., Radhakrishnan, A., Rand, K., Vahlenkamp, H., Wilson, C., Zadeh, N. T., Dunne, J. P., Dussin, R., Horowitz, L. W., Krasting, J. P., Lin, P., Malyshev, S., Naik, V., Ploshay, J., Shevliakova, E., Silvers, L., Stock, C., Winton, M., and Zeng, Y.: NOAA-GFDL GFDL-ESM4 model output prepared for CMIP6 ScenarioMIP ssp245, https://doi.org/10.22033/ESGF/CMIP6.8686, 2018.

Jones, G.: MOHC HadGEM3-GC31-LL model output prepared for CMIP6 DAMIP hist-GHG, https://doi.org/10.22033/ESGF/CMIP6.6051, 2019a.

Jones, G.: MOHC HadGEM3-GC31-LL model output prepared for CMIP6 DAMIP hist-aer, https://doi.org/10.22033/ESGF/CMIP6.6052, 2019b.

Jones, G.: MOHC HadGEM3-GC31-LL model output prepared for CMIP6 DAMIP hist-nat, https://doi.org/10.22033/ESGF/CMIP6.6059, 2019c.

Knutti, R., Rugenstein, M., and Hegerl, G.: Beyond equilibrium climate sensitivity, Nature Geosci., 10, 727–736, https://doi.org/10.1038/ngeo3017, 2017.

Krasting, J. P., John, J. G., Blanton, C., McHugh, C., Nikonov, S., Radhakrishnan, A., Rand, K., Zadeh, N. T., Balaji, V., Durachta, J., Dupuis, C., Menzel, R., Robinson, T., Underwood, S., Vahlenkamp, H., Dunne, K. A., Gauthier, P. P., Ginoux, P., Griffies, S. M., Hallberg, R., Harrison, M., Hurlin, W., Malyshev, S., Naik, V., Paulot, F., Paynter, D. J., Ploshay, J., Reichl, B. G., Schwarzkopf, D. M., Seman, C. J., Silvers, L., Wyman, B., Zeng, Y., Adcroft, A., Dunne, J. P., Dussin, R., Guo, H., He, J., Held, I. M., Horowitz, L. W., Lin, P., Milly, P., Shevliakova, E., Stock, C., Winton, M., Wittenberg, A. T., Xie, Y., and Zhao, M.: NOAA-GFDL GFDL-ESM4 model output prepared for CMIP6 CMIP historical, https://doi.org/10.22033/ESGF/CMIP6.8597, 2018.

Lee, J.-Y., Marotzke, J., Bala, G., Cao, L., Corti, S., Dunne, J., Engelbrecht, F., Fischer, E., Fyfe, J., Jones, C., Maycock, A., Mutemi, J., Ndiaye, O., Panickal, S., and Zhou, T.: Future Global Climate: Scenario-Based Projections and Near-Term Information, in: Climate Change 2021: The Physical Science Basis. Contribution of Working Group I to the Sixth Assessment Report of the Intergovernmental Panel on Climate Change, edited by Masson-Delmotte, V., Zhai, P., Pirani, A., Connors, S., Péan, C., Berger, S., Caud, N., Chen, Y., Goldfarb, L., Gomis, M., Huang, M., Leitzell, K., Lonnoy, E., Matthews, J., Maycock, T., Waterfield, T., Yelekçi, O., Yu, R., and Zhou, B., p. 553–672, Cambridge University Press, Cambridge, United Kingdom and New York, NY, USA, https://doi.org/10.1017/9781009157896.006, 2021.

Li, L.: CAS FGOALS-g3 model output prepared for CMIP6 CMIP historical, https://doi.org/10.22033/ESGF/CMIP6.3356, 2019.

https://doi.org/10.5194/egusphere-2023-2427
Preprint. Discussion started: 18 December 2023

Li, L.: CAS FGOALS-g3 model output prepared for CMIP6 DAMIP hist-GHG, https://doi.org/10.22033/ESGF/CMIP6.3321, 2020a.

Li, L.: CAS FGOALS-g3 model output prepared for CMIP6 DAMIP hist-aer, https://doi.org/10.22033/ESGF/CMIP6.3323, 2020b.

Li, L.: CAS FGOALS-g3 model output prepared for CMIP6 DAMIP hist-nat, https://doi.org/10.22033/ESGF/CMIP6.3330, 2020c.

Li, L.: CAS FGOALS-g3 model output prepared for CMIP6 ScenarioMIP ssp245, 2020d.

Li, L., Yu, Y., Tang, Y., Lin, P., Xie, J., Song, M., Dong, L., Zhou, T., Liu, L., Wang, L., Pu, Y., Chen, X., Chen, L., Xie, Z., Liu, H., Zhang, L., Huang, X., Feng, T., Zheng, W., Xia, K., Liu, H., Liu, J., Wang, Y., Wang, L., Jia, B., Xie, F., Wang, B., Zhao, S., Yu, Z., Zhao, B., and Wei, J.: The Flexible Global Ocean-Atmosphere-Land System Model Grid-Point Version 3 (FGOALS-g3): description and evaluation, Journal of Advances in Modeling Earth Systems, 12, e2019MS002 012, https://doi.org/https://doi.org/10.1029/2019MS002012, e2019MS002012 2019MS002012, 2020.

Meehl, G. A., Senior, C. A., Eyring, V., Flato, G., Lamarque, J.-F., Stouffer, R. J., Taylor, K. E., and Schlund, M.: Context for interpreting equilibrium climate sensitivity and transient climate response from the CMIP6 Earth system models, Science Advances, 6, eaba1981, https://doi.org/10.1126/sciadv.aba1981, 2020.

Morice, C. P., Kennedy, J. J., Rayner, N. A., Winn, J. P., Hogan, E., Killick, R. E., Dunn, R. J. H., Osborn, T. J., Jones, P. D., and Simpson, I. R.: An updated assessment of near-surface temperature change from 1850: The HadCRUT5 data set, Journal of Geophysical Research: Atmospheres, 126, e2019JD032 361, https://doi.org/https://doi.org/10.1029/2019JD032361, e2019JD032361 2019JD032361, 2021.

NASA/GISS: NASA-GISS GISS-E2.1G model output prepared for CMIP6 CMIP historical, https://doi.org/10.22033/ESGF/CMIP6.7127, 2018a.

NASA/GISS: NASA-GISS GISS-E2.1G model output prepared for CMIP6 DAMIP hist-GHG, https://doi.org/10.22033/ESGF/CMIP6.7079, 2018b.

NASA/GISS: NASA-GISS GISS-E2.1G model output prepared for CMIP6 DAMIP hist-aer, https://doi.org/10.22033/ESGF/CMIP6.7081, 2018c.

NASA/GISS: NASA-GISS GISS-E2.1G model output prepared for CMIP6 DAMIP hist-nat, 2018d.

Qin, Y., Zheng, X., Klein, S. A., Zelinka, M. D., Ma, P.-L., Golaz, J.-C., and Xie, S.: Causes of reduced climate sensitivity in E3SM from version 1 to version 2, ESS Open Archive, https://doi.org/10.22541/essoar.168677205.57448605/v1, 2023.

Ridley, J., Menary, M., Kuhlbrodt, T., Andrews, M., and Andrews, T.: MOHC HadGEM3-GC31-LL model output prepared for CMIP6 CMIP historical, https://doi.org/10.22033/ESGF/CMIP6.6109, 2019.

Seland, Ø., Bentsen, M., Oliviè, D. J. L., Toniazzo, T., Gjermundsen, A., Graff, L. S., Debernard, J. B., Gupta, A. K., He, Y., Kirkevåg, A., Schwinger, J., Tjiputra, J., Aas, K. S., Bethke, I., Fan, Y., Griesfeller, J., Grini, A., Guo, C., Ilicak, M., Karset, I. H. H., Landgren, O. A., Liakka, J., Moseid, K. O., Nummelin, A., Spensberger, C., Tang, H., Zhang, Z., Heinze, C., Iversen, T., and Schulz, M.: NCC NorESM2-LM model output prepared for CMIP6 CMIP historical, https://doi.org/10.22033/ESGF/CMIP6.8036, 2019a.

Seland, Ø., Bentsen, M., Oliviè, D. J. L., Toniazzo, T., Gjermundsen, A., Graff, L. S., Debernard, J. B., Gupta, A. K., He, Y., Kirkevåg, A., Schwinger, J., Tjiputra, J., Aas, K. S., Bethke, I., Fan, Y., Griesfeller, J., Grini, A., Guo, C., Ilicak, M., Karset, I. H. H., Landgren, O. A., Liakka, J., Moseid, K. O., Nummelin, A., Spensberger, C., Tang, H., Zhang, Z., Heinze, C., Iversen, T., and Schulz, M.: NCC NorESM2-LM model output prepared for CMIP6 DAMIP hist-GHG, https://doi.org/10.22033/ESGF/CMIP6.7966, 2019b.

Seland, Ø., Bentsen, M., Oliviè, D. J. L., Toniazzo, T., Gjermundsen, A., Graff, L. S., Debernard, J. B., Gupta, A. K., He, Y., Kirkevåg, A., Schwinger, J., Tjiputra, J., Aas, K. S., Bethke, I., Fan, Y., Griesfeller, J., Grini, A., Guo, C., Ilicak, M., Karset, I. H. H., Landgren, O. A., Liakka, J., Moseid, K. O., Nummelin, A., Spensberger, C., Tang, H., Zhang, Z., Heinze, C., Iversen, T., and Schulz, M.: NCC NorESM2-LM model output prepared for CMIP6 DAMIP hist-aer, https://doi.org/10.22033/ESGF/CMIP6.7969, 2019c.

https://doi.org/10.5194/egusphere-2023-2427
Preprint. Discussion started: 18 December 2023

Seland, Ø., Bentsen, M., Oliviè, D. J. L., Toniazzo, T., Gjermundsen, A., Graff, L. S., Debernard, J. B., Gupta, A. K., He, Y., Kirkevåg, A., Schwinger, J., Tjiputra, J., Aas, K. S., Bethke, I., Fan, Y., Griesfeller, J., Grini, A., Guo, C., Ilicak, M., Karset, I. H. H., Landgren, O. A., Liakka, J., Moseid, K. O., Nummelin, A., Spensberger, C., Tang, H., Zhang, Z., Heinze, C., Iversen, T., and Schulz, M.: NCC NorESM2-LM model output prepared for CMIP6 DAMIP hist-nat, https://doi.org/10.22033/ESGF/CMIP6.7979, 2019d.

Seland, Ø., Bentsen, M., Oliviè, D. J. L., Toniazzo, T., Gjermundsen, A., Graff, L. S., Debernard, J. B., Gupta, A. K., He, Y., Kirkevåg, A., Schwinger, J., Tjiputra, J., Aas, K. S., Bethke, I., Fan, Y., Griesfeller, J., Grini, A., Guo, C., Ilicak, M., Karset, I. H. H., Landgren, O. A., Liakka, J., Moseid, K. O., Nummelin, A., Spensberger, C., Tang, H., Zhang, Z., Heinze, C., Iversen, T., and Schulz, M.: NCC NorESM2-LM model output prepared for CMIP6 ScenarioMIP ssp245, https://doi.org/10.22033/ESGF/CMIP6.8253, 2019e.

Shiogama, H.: MIROC MIROC6 model output prepared for CMIP6 DAMIP hist-GHG, https://doi.org/10.22033/ESGF/CMIP6.5578, 2019a.

Shiogama, H.: MIROC MIROC6 model output prepared for CMIP6 DAMIP hist-aer, https://doi.org/10.22033/ESGF/CMIP6.5579, 2019b.

Shiogama, H.: MIROC MIROC6 model output prepared for CMIP6 DAMIP hist-nat, https://doi.org/10.22033/ESGF/CMIP6.5583, 2019c.

Shiogama, H., Abe, M., and Tatebe, H.: MIROC MIROC6 model output prepared for CMIP6 ScenarioMIP ssp245, https://doi.org/10.22033/ESGF/CMIP6.5746, 2019.

Smith, C. J. and Forster, P. M.: Suppressed late-20th century warming in CMIP6 models explained by forcing and feedbacks, Geophysical Research Letters, 48, e2021GL094 948, https://doi.org/https://doi.org/10.1029/2021GL094948, e2021GL094948 2021GL094948, 2021.

Stone, D. A., Allen, M. R., Selten, F., Kliphuis, M., and Stott, P. A.: The detection and attribution of climate change Using an ensemble of opportunity, Journal of Climate, 20, 504–516, https://doi.org/https://doi.org/10.1175/JCLI3966.1, 2007a.

Stone, D. A., Allen, M. R., and Stott, P. A.: A multimodel update on the detection and attribution of global surface warming, Journal of Climate, 20, 517–530, https://doi.org/https://doi.org/10.1175/JCLI3964.1, 2007b.

Swart, N. C., Cole, J. N., Kharin, V. V., Lazare, M., Scinocca, J. F., Gillett, N. P., Anstey, J., Arora, V., Christian, J. R., Jiao, Y., Lee, W. G., Majaess, F., Saenko, O. A., Seiler, C., Seinen, C., Shao, A., Solheim, L., von Salzen, K., Yang, D., Winter, B., and Sigmond, M.: CCCma CanESM5 model output prepared for CMIP6 CMIP historical, https://doi.org/10.22033/ESGF/CMIP6.3610, 2019a.

Swart, N. C., Cole, J. N., Kharin, V. V., Lazare, M., Scinocca, J. F., Gillett, N. P., Anstey, J., Arora, V., Christian, J. R., Jiao, Y., Lee, W. G., Majaess, F., Saenko, O. A., Seiler, C., Seinen, C., Shao, A., Solheim, L., von Salzen, K., Yang, D., Winter, B., and Sigmond, M.: CCCma CanESM5 model output prepared for CMIP6 DAMIP hist-GHG, https://doi.org/10.22033/ESGF/CMIP6.3596, 2019b.

Swart, N. C., Cole, J. N., Kharin, V. V., Lazare, M., Scinocca, J. F., Gillett, N. P., Anstey, J., Arora, V., Christian, J. R., Jiao, Y., Lee, W. G., Majaess, F., Saenko, O. A., Seiler, C., Seinen, C., Shao, A., Solheim, L., von Salzen, K., Yang, D., Winter, B., and Sigmond, M.: CCCma CanESM5 model output prepared for CMIP6 DAMIP hist-aer, https://doi.org/10.22033/ESGF/CMIP6.3597, 2019c.

Swart, N. C., Cole, J. N., Kharin, V. V., Lazare, M., Scinocca, J. F., Gillett, N. P., Anstey, J., Arora, V., Christian, J. R., Jiao, Y., Lee, W. G., Majaess, F., Saenko, O. A., Seiler, C., Seinen, C., Shao, A., Solheim, L., von Salzen, K., Yang, D., Winter, B., and Sigmond, M.: CCCma CanESM5 model output prepared for CMIP6 DAMIP hist-nat, https://doi.org/10.22033/ESGF/CMIP6.3601, 2019d.

Swart, N. C., Cole, J. N., Kharin, V. V., Lazare, M., Scinocca, J. F., Gillett, N. P., Anstey, J., Arora, V., Christian, J. R., Jiao, Y., Lee, W. G., Majaess, F., Saenko, O. A., Seiler, C., Seinen, C., Shao, A., Solheim, L., von Salzen, K., Yang, D., Winter, B., and Sigmond, M.: CCCma CanESM5 model output prepared for CMIP6 ScenarioMIP ssp245, https://doi.org/10.22033/ESGF/CMIP6.3685, 2019e.

Szopa, S., Naik, V., Adhikary, B., Artaxo, P., Berntsen, T., Collins, W., Fuzzi, S., Gallardo, L., Kiendler-Scharr, A., Klimont, Z., Liao, H., Unger, N., and Zanis, P.: Short-Lived Climate Forcers, in: Climate Change 2021: The Physical Science Basis. Contribution of Working Group I to the Sixth Assessment Report of the Intergovernmental Panel on Climate Change, edited by Masson-Delmotte, V., Zhai, P., Pirani, A., Connors, S., Péan, C., Berger, S., Caud, N., Chen, Y., Goldfarb, L., Gomis, M., Huang, M., Leitzell, K., Lonnoy, E., Matthews,

https://doi.org/10.5194/egusphere-2023-2427
Preprint. Discussion started: 18 December 2023

J., Maycock, T., Waterfield, T., Yelekçi, O., Yu, R., and Zhou, B., p. 817–922, Cambridge University Press, Cambridge, United Kingdom and New York, NY, USA, https://doi.org/10.1017/9781009157896.008, 2021.

Tatebe, H. and Watanabe, M.: MIROC MIROC6 model output prepared for CMIP6 CMIP historical, https://doi.org/10.22033/ESGF/CMIP6.5603, 2018.

Voldoire, A.: CMIP6 simulations of the CNRM-CERFACS based on CNRM-CM6-1 model for CMIP experiment historical, https://doi.org/10.22033/ESGF/CMIP6.4066, 2018.

Voldoire, A.: CNRM-CERFACS CNRM-CM6-1 model output prepared for CMIP6 DAMIP hist-GHG, https://doi.org/10.22033/ESGF/CMIP6.4043, 2019a.

Voldoire, A.: CNRM-CERFACS CNRM-CM6-1 model output prepared for CMIP6 DAMIP hist-aer, https://doi.org/10.22033/ESGF/CMIP6.4044, 2019b.

Voldoire, A.: CNRM-CERFACS CNRM-CM6-1 model output prepared for CMIP6 DAMIP hist-nat, https://doi.org/10.22033/ESGF/CMIP6.4048, 2019c.

Voldoire, A.: CNRM-CERFACS CNRM-CM6-1 model output prepared for CMIP6 ScenarioMIP ssp245, https://doi.org/10.22033/ESGF/CMIP6.4189, 2019d.

Watson-Parris, D. and Smith, C.: Large uncertainty in future warming due to aerosol forcing, Nature Climate Change, 12, 1111–1113, https://doi.org/10.1038/s41558-022-01516-0, 2022.

Wu, T., Chu, M., Dong, M., Fang, Y., Jie, W., Li, J., Li, W., Liu, Q., Shi, X., Xin, X., Yan, J., Zhang, F., Zhang, J., Zhang, L., and Zhang, Y.: BCC BCC-CSM2MR model output prepared for CMIP6 CMIP historical, https://doi.org/10.22033/ESGF/CMIP6.2948, 2018.

Wu, T., Chu, M., Dong, M., Fang, Y., Jie, W., Li, J., Li, W., Liu, Q., Shi, X., Xin, X., Yan, J., Zhang, F., Zhang, J., Zhang, L., and Zhang, Y.: BCC BCC-CSM2MR model output prepared for CMIP6 DAMIP hist-GHG, https://doi.org/10.22033/ESGF/CMIP6.2924, 2019a.

Wu, T., Chu, M., Dong, M., Fang, Y., Jie, W., Li, J., Li, W., Liu, Q., Shi, X., Xin, X., Yan, J., Zhang, F., Zhang, J., Zhang, L., and Zhang, Y.: BCC BCC-CSM2MR model output prepared for CMIP6 DAMIP hist-aer, https://doi.org/10.22033/ESGF/CMIP6.2925, 2019b.

Wu, T., Chu, M., Dong, M., Fang, Y., Jie, W., Li, J., Li, W., Liu, Q., Shi, X., Xin, X., Yan, J., Zhang, F., Zhang, J., Zhang, L., and Zhang, Y.: BCC BCC-CSM2MR model output prepared for CMIP6 DAMIP hist-nat, https://doi.org/10.22033/ESGF/CMIP6.2929, 2019c.

Xin, X., Wu, T., Shi, X., Zhang, F., Li, J., Chu, M., Liu, Q., Yan, J., Ma, Q., and Wei, M.: BCC BCC-CSM2MR model output prepared for CMIP6 ScenarioMIP ssp245, https://doi.org/10.22033/ESGF/CMIP6.3030, 2019.

Yukimoto, S., Kawai, H., Koshiro, T., Oshima, N., Yoshida, K., Urakawa, S., Tsujino, H., Deushi, M., Tanaka, T., Hosaka, M., Yabu, S., Yoshimura, H., Shindo, E., Mizuta, R., Obata, A., Adachi, Y., and Ishii, M.: The Meteorological Research Institute Earth System Model Version 2.0, MRI-ESM2.0: Description and basic evaluation of the physical component, Journal of the Meteorological Society of Japan Ser. II, https://doi.org/10.2151/jmsj.2019-051, 2019a.

Yukimoto, S., Koshiro, T., Kawai, H., Oshima, N., Yoshida, K., Urakawa, S., Tsujino, H., Deushi, M., Tanaka, T., Hosaka, M., Yoshimura, H., Shindo, E., Mizuta, R., Ishii, M., Obata, A., and Adachi, Y.: MRI MRI-ESM2.0 model output prepared for CMIP6 DAMIP hist-GHG, https://doi.org/10.22033/ESGF/CMIP6.6820, 2019b.

Yukimoto, S., Koshiro, T., Kawai, H., Oshima, N., Yoshida, K., Urakawa, S., Tsujino, H., Deushi, M., Tanaka, T., Hosaka, M., Yoshimura, H., Shindo, E., Mizuta, R., Ishii, M., Obata, A., and Adachi, Y.: MRI MRI-ESM2.0 model output prepared for CMIP6 DAMIP hist-aer, https://doi.org/10.22033/ESGF/CMIP6.6821, 2019c.

https://doi.org/10.5194/egusphere-2023-2427
Preprint. Discussion started: 18 December 2023

Yukimoto, S., Koshiro, T., Kawai, H., Oshima, N., Yoshida, K., Urakawa, S., Tsujino, H., Deushi, M., Tanaka, T., Hosaka, M., Yoshimura, H., Shindo, E., Mizuta, R., Ishii, M., Obata, A., and Adachi, Y.: MRI MRI-ESM2.0 model output prepared for CMIP6 DAMIP hist-nat, https://doi.org/10.22033/ESGF/CMIP6.6825, 2019d.

Yukimoto, S., Koshiro, T., Kawai, H., Oshima, N., Yoshida, K., Urakawa, S., Tsujino, H., Deushi, M., Tanaka, T., Hosaka, M., Yoshimura, H., Shindo, E., Mizuta, R., Ishii, M., Obata, A., and Adachi, Y.: MRI MRI-ESM2.0 model output prepared for CMIP6 ScenarioMIP ssp245, https://doi.org/10.22033/ESGF/CMIP6.6910, 2019e.

Ziehn, T., Chamberlain, M., Lenton, A., Law, R., Bodman, R., Dix, M., Wang, Y., Dobrohotoff, P., Srbinovsky, J., Stevens, L., Vohralik, P., Mackallah, C., Sullivan, A., O'Farrell, S., and Druken, K.: CSIRO ACCESS-ESM1.5 model output prepared for CMIP6 CMIP historical, https://doi.org/10.22033/ESGF/CMIP6.4272, 2019a.

Ziehn, T., Chamberlain, M., Lenton, A., Law, R., Bodman, R., Dix, M., Wang, Y., Dobrohotoff, P., Srbinovsky, J., Stevens, L., Vohralik, P., Mackallah, C., Sullivan, A., O'Farrell, S., and Druken, K.: CSIRO ACCESS-ESM1.5 model output prepared for CMIP6 ScenarioMIP ssp245, https://doi.org/10.22033/ESGF/CMIP6.4322, 2019b.

Ziehn, T., Dix, M., Mackallah, C., Chamberlain, M., Lenton, A., Law, R., Druken, K., and Ridzwan, S. M.: CSIRO ACCESS-ESM1.5 model output prepared for CMIP6 DAMIP hist-GHG, https://doi.org/10.22033/ESGF/CMIP6.14366, 2020a.

Ziehn, T., Dix, M., Mackallah, C., Chamberlain, M., Lenton, A., Law, R., Druken, K., and Ridzwan, S. M.: CSIRO ACCESS-ESM1.5 model output prepared for CMIP6 DAMIP hist-aer, https://doi.org/10.22033/ESGF/CMIP6.14370, 2020b.

Ziehn, T., Dix, M., Mackallah, C., Chamberlain, M., Lenton, A., Law, R., Druken, K., and Ridzwan, S. M.: CSIRO ACCESS-ESM1.5 model output prepared for CMIP6 DAMIP hist-nat, https://doi.org/10.22033/ESGF/CMIP6.14378, 2020c.